Journal of
Ceramic Science
and Technology

J. Ceram. Sci. Tech., 02 [02] 111-118 (2011)
DOI: 10.4416/JCST2011-00007
available online at: http://www.ceramic-science.com

Manufacturing, Analysis and Modelling of Porous Si-SiC Ceramics Derived by Oxidation from C/C-Si-SiC Composites

V.K. Srivastava*[1], W. Krenkel[2], V.J.A. D'Souza[1] and H.W. Mucha[2]

[1]Banaras Hindu University, Institute of Technology, Department of Mechanical Engineering, Varanasi, India

[2]University of Bayreuth, Department of Ceramic Materials Engineering, Bayreuth, Germany

received November 7, 2010; received in revised form March 4, 2011; accepted March 11, 2011

Abstract

Novel porous Si-SiC ceramics are derived by the oxidation of C/C-Si-SiC fibre matrix composites. The correlated mass loss and obtained open porosity depend on the temperature and holding times of the oxidation process. Microstructure and phase analyses of the Si-SiC composites are performed and supplemented with experimental determinations of the open porosity, the pore size distribution and surface area. These macroscopic properties are influenced by the parameters of the oxidation process. Material parameters like the fibre alignment (weave style resp. fibre length) and phenolic resin type (resol and novolac) are considered as well. The experimental findings serve as a basis for modelling the open porosity. The open porosity and its pore size distribution are determined theoretically on this model basis and validated with the experimental results.

Keywords: C/C-SiC composite, Si-SiC porous ceramic, oxidation, open porosity

I. Introduction

C/C-SiC composites exhibit extraordinary mechanical and thermal characteristics such as low density, high strength-to-weight ratio, and high resistance to wear or retention of mechanical properties at high temperature. Extensive applications exist in the aerospace and aeronautics industries for rocket nozzles and re-entry thermal protection shields for space vehicles, in the automotive industry for ceramic brake discs, heat insulating materials and various other structural applications. Further, SiC-based ceramics are known to exhibit excellent oxidation characteristics owing to the formation of a protective silica scale, which slows down the oxidation rate as long as the oxidation conditions remain those of the passive oxidation regime of SiC. Significant research is going on in the development of porous materials for different applications. These porous materials include graphite/carbon foam, ceramic foam, porous conducting paper for electrodes of fuel cells, etc. However, the present work is aimed at the manufacture and characterization of a novel material, styled as "Si-SiC porous ceramic", derived from C/C-SiC composites that exhibit superior performance compared to conventional porous materials [1–5].

Silicon infiltrates into the segmentation cracks arising during pyrolysis of carbon-fibre-reinforced plastic composites (CFRP) and forms layers of protective segments over the carbon fibres, retarding the oxidation of the C/C-SiC composite when this is exposed to high-temperature environments. However, the carbon fibres that run through the C/C-SiC laminate are not completely covered by the silicon carbide/free silicon in the longitudinal direction of the fibres. The realization of the idea was also derived from the fact that differences exist in the oxidation temperatures between carbon, silicon carbide and free silicon [6–9]. The above-mentioned facts concerning C/C-SiC composites are exploited to obtain such a material. Hence, a controlled oxidation of the C/C-SiC composite in an oxidizing atmosphere should result in the oxidation of the carbon fibres, leaving behind only a network of channels resulting from the depletion of carbon throughout the entire composite to form a highly porous structure. Considering the oxidation of the carbon matrix as well, the open porosity obtained should be significantly high [10, 11].

The C/C-SiC composites converted to Si-SiC ceramics consist of C/C-segments surrounded by Si/SiC walls. These protective segments consist of silicon carbide and free silicon and prevent the oxidation of the C/C blocks within the C/C-SiC composite in oxidative environments at high temperature [12, 13].

Nevertheless, controlled oxidation of the C/C-SiC composite in an oxidizing atmosphere is possible and results in the selective oxidation/depletion of the areas containing carbon fibres. A multiply connected network of channels is formed throughout the entire composite and results in a highly porous, open material structure. The oxidation temperatures of carbon, silicon carbide and free silicon differ.

Selected C/C-SiC composites obtained with the liquid silicon infiltration technique act as the starting materials for controlled oxidation and transformation to porous Si-

* Corresponding author: vijayks210@gmail.com

SiC ceramic. The Liquid Silicon Infiltration (LSI) process, a low-cost manufacturing route developed at the German Aerospace Center (DLR), comprises three main processing steps [1].

Carbon fibres (short fibres or woven fabrics) are stacked and impregnated with phenolic resin (novolac or resol type) and cured, leading to carbon-fibre-reinforced plastics (CFRP). The open porosity of the CFRP is roughly at about 1 % at this step. The CFRPs are thermally treated in an inert atmosphere up to 900 °C or 1650 °C, which leads to shrinkage and transformation of the former polymer to a carbon matrix. That process is correlated with the generation of cracking products, mainly CO, CO_2 and H_2O gases, and creates the carbon/carbon composites. Their interconnecting pore structure consists of translaminar crack patterns and ranges at about 20 % at this stage.

The final C/C-SiC composite manufacturing step is the infiltration of molten silicon into the cracks/pores of the porous C/C composite. Infiltration paths tend to be along the direction of the fibres. The silicon reacts with adjacent carbon to form silicon carbide. In case of 2-D reinforcements and a strong fibre/matrix bonding, layers of SiC are generated around those C/C-segments and protect the interior against oxidation. The generation of the porous Si-SiC ceramics requires a supplementary oxidation step following the LSI process. The C/C-SiC ceramics are oxidized at controlled temperatures in ambient air/oxygen atmosphere for a pre-defined duration. The applied oxidation temperatures and main decomposition products are shown in Table 1. The parameters of the oxidation process are chosen to prevent the formation of silica (SiO_2), an amorphous phase, which can cause degradation of the properties of the porous Si-SiC ceramic. At low temperatures the oxidation is controlled by the chemical reaction rate and at higher temperatures by the diffusion of the involved gases from and to the oxidation sites.

In the present work, manufacturing, modelling and analysis of porous Si-SiC ceramics derived by oxidation of C/C-Si-SiC composites will be presented with the variation of oxidation temperature from 750 to 1200 °C.

Table 1: Constituents of C/C-SiC ceramics along with their oxidation temperatures and oxidation products.

Constituent	Oxidation temperature (°C)	Oxidation products
Carbon (C)	Above 400 – 450 °C	CO_2
Silicon carbide (SiC)	Rapidly above 1200 °C	SiO_2, CO_2
Silicon (Si)	Rapidly above 870 °C	SiO_2

II. Experimental

(1) Thermogravimetric analysis

The samples are usually sized to dimensions of about 6 mm × 6 mm × 3 mm and subjected to a controlled heating/cooling regime under a dynamic air flow of 5.0 l/min in a thermogravimetric set-up.

The thermal behaviour of resol and novolac type resins as matrices are investigated by controlling the weight losses and the obtained porosity. Experimentally for each selected peak temperature, a virgin sample of the same starting material (resol or novolac-based) passed a full thermal oxidation cycle before the mass is weighted and the porosity determined with a helium-gas pycnometer. This cycle consists of heating the sample from room temperature to the selected peak temperature in a regular furnace in a static, ambient atmosphere at a fixed heating rate (10 K/min). After the peak temperature has been held for 2 h, cooling down at a rate of 10 K/min follows. Twill-weave-based virgin C/C-SiC composites are used with a size of about 20 mm × 20 mm × 3 mm.

(2) Phase analysis

C/C-SiC composites of novolac resin, twill-weave type are oxidized at 1200 °C for 24 h and then microscopically investigated. The integral elemental composition all over the analysis is determined with EDX. X-ray diffraction (XRD) method is performed on the samples after exposing them to oxidation at 1200 °C for different times. Large numbers of pores are formed at 1200 °C so that silicon phase is predominantly present in the sample. C/C-SiC composites exposed to an oxidation at 800 °C to 1200 °C for different durations of time are discussed representatively.

(3) Scanning electron microscopy

Novolac- and resol-derived C-fabric (twill)-reinforced and novolac-based C-short fibre-reinforced C/C-SiC composites that have already undergone oxidation treatment (800 °C to 1200 °C for 2 h) are subjects of the microscope studies. Owing to the large depth of focus, scanning electron microscopy (SEM) is better suited to reveal the material characteristics than optical microscopy. The SEM images were captured in secondary electron mode and in the back-scatter electron mode. The back-scatter mode more clearly reveals elemental silicon patches embedded in SiC surroundings.

(4) Computer tomography analysis

A 3-dimensional reconstruction of the structure of porous Si-SiC samples (novolac, twill) is performed using computer tomography (CT) and 3-dimensional image analysis software. It visualizes impressively the location and shape of the channels created during oxidation at 1200 °C and 2 h of exposure.

The porosity of oxidized samples is determined with helium-gas pycnometry. The porosity of all the samples is also determined with the Archimedes method in accordance with the DIN EN 632 – 2 standard. The obtained porosities remain below those measured by the helium-gas pycnometry by about 3 – 6 %. Archimedes densities range from 0.8 g/cm³ to 1.0 g/cm³.

III. Results and Discussion

(1) Thermal behaviour of resol- and novolac-based composites

The thermal behaviour of C/C-SiC composites (resol- or novolac-type resin) is used to obtain the mass loss with the variation of time at the range of 850 °C as shown in Fig. 1.

The time-temperature curve (TTC) is investigated with C/C-SiC composites; this covers the temperature range up to 850 °C with a heating rate of 3 K/min and is kept constant for a period of 10 h. Then, cooling takes place at a rate of 3 K/min. The time dependence of the occurring mass losses is investigated. The cumulative losses range from 55 % to 63 % (Fig. 1) and show little differences between the resin types (resol or novolac) and the type of fibre arrangement (woven fabrics or short fibres). No changes of mass are observed after longer times and at 850 °C when the carbon is already completely removed.

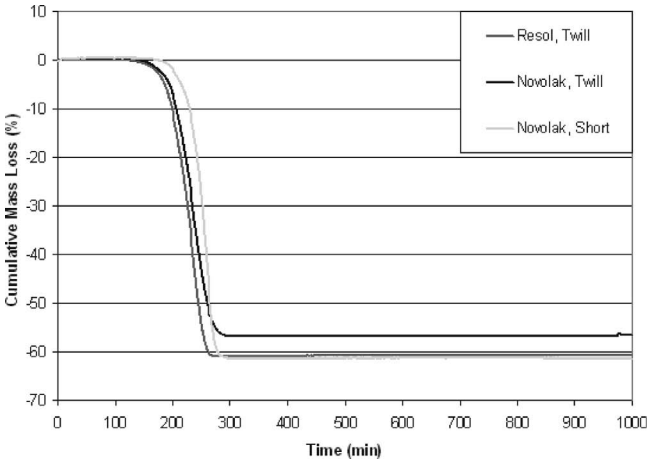

Fig. 1: Variation of the mass loss percentage of C/C-SiC composites as a function of time.

The temperature dependence of the incremental mass losses of C/C-SiC is shown in Fig. 2. They maximize at around 750 – 800 °C. The depletion of carbon inside the samples causes the mass loss to decline even at higher temperatures. The peak temperature of the incremental loss and the temperature range of these losses can be attributed to differences in the sample size and the actual amount of carbon available.

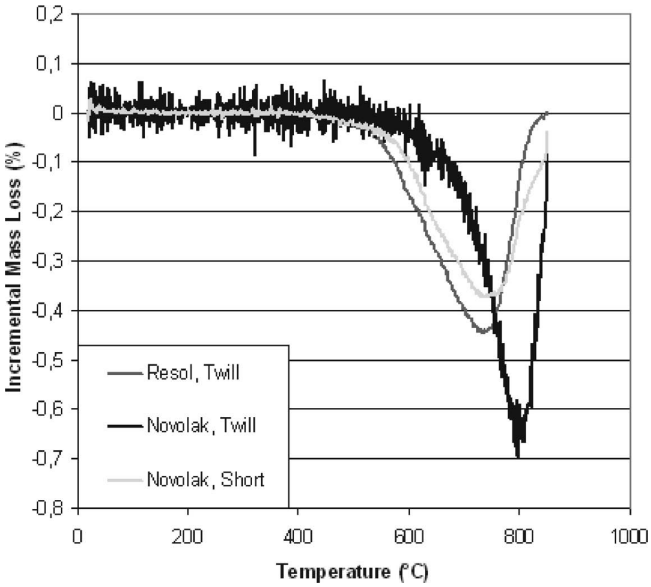

Fig. 2: Variation of the mass loss percentage of C/C-SiC composites as a function of temperature.

The results of the single experiments are compiled in Figs. 3 and 4. The temperature dependence of the mass loss (Fig. 3) indicates declining (incremental) mass losses at higher temperatures. No significant differences in mass loss patterns occur between novolac and resol, except the fact that novolac shows slightly higher mass losses compared to resol.

The investigations of the temperature dependence of the obtained open porosity for oxidized twill-weave-based C/C-SiC composites show a slightly higher porosity in novolac-derived C/C-SiC composites compared to resol-based samples (Fig. 4) at lower temperature. More closed pores are present in the novolac (a powder resin)-based C/C-SiC compared to the resol-based composites. These closed pores open during earlier oxidation steps and convert to open porosity, which is detected with the He-pycnometer. The systematic influence of the resin type used for processing the C/C-SiC composites on the porosity of Si-SiC composites nevertheless is just marginal.

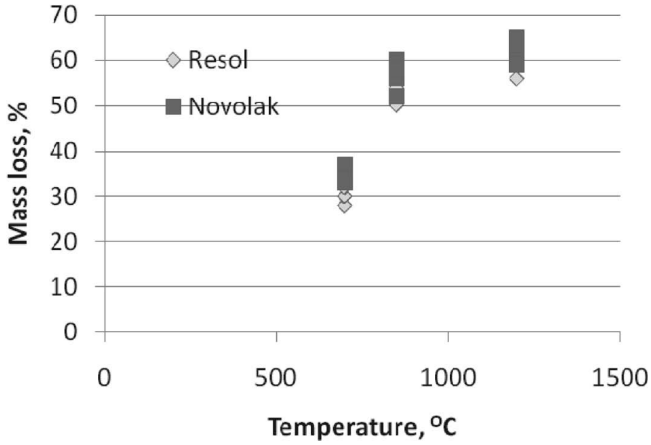

Fig. 3: Variation of the mass loss of oxidized-twill-weave-derived C/C-SiC composites as a function of temperature.

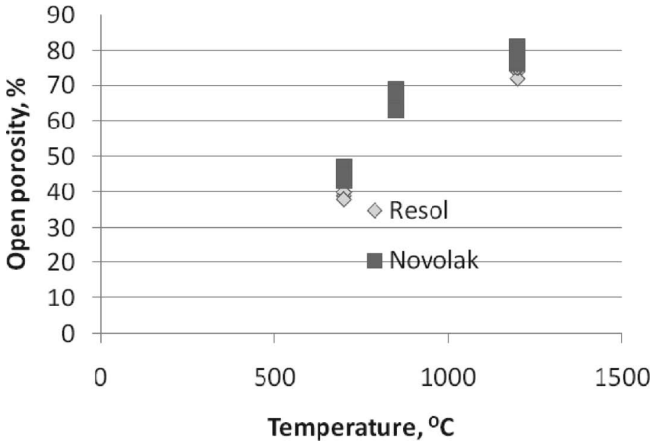

Fig. 4: Variation of the open porosity of oxidized-twill-weave-derived C/C-SiC composites as a function of temperature.

The influence of the fibre arrangement (twill weave or short fibre) on the thermal degradation, i.e. mass loss and open porosity under conditions is shown in Figs. 5 and 6. The temperature dependence of the mass loss (Fig. 5) clearly shows that twill-weave-based samples are more prone to fast thermal degradation than the short fibre samples. The reason is the segmented and symmetric structure of the twill-weave-based composites which makes all parts of the sample accessible to oxygen in a shorter time than

possible in the less well-organized short-fibre-derived composites. Short-fibre-based composites possess a highly random fibre arrangement, which kinetically delays oxidation.

The influence of temperature on the open porosity (Fig. 6) is related to mass losses. Compared to short-fibre materials, twill-weave-based composites tend to facilitate gas transport through the sample with increasing temperature by accessing closed pores some time before the conversion of carbon is completed.

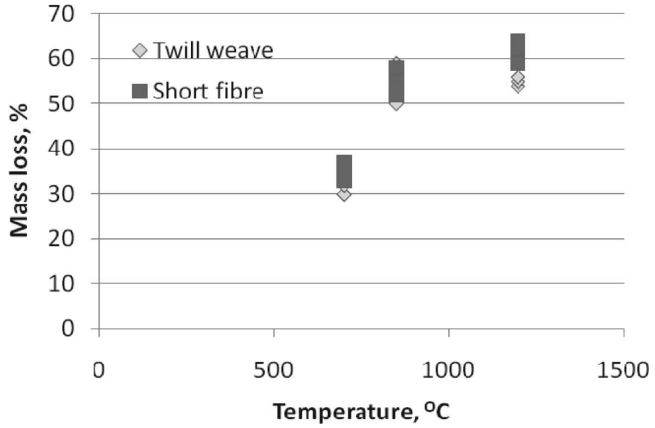

Fig. 5: Variation of the mass loss of oxidized-novolac-resin-derived C/C-SiC composites as a function of temperature.

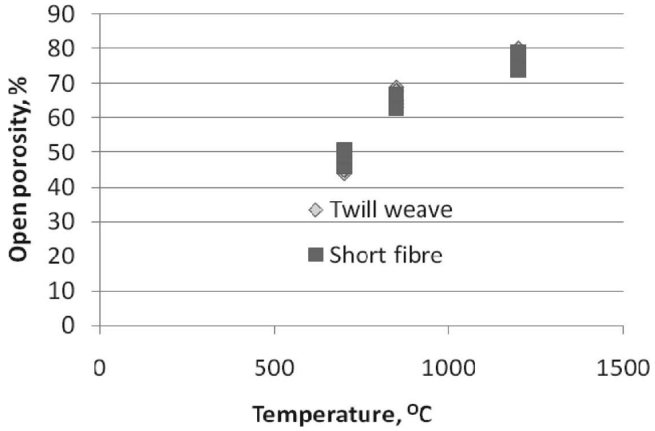

Fig. 6: Variation of the open porosity of oxidized-novolac-resin-derived C/C-SiC composites as a function of temperature.

(2) Phase analyses

A representative area is shown in Fig. 7 (a), whereas Fig. 7 (b) shows the elemental spectrum averaged over the analysis area shown in Fig. 7 (a), with carbon, oxygen and silicon signals. The silicon intensity is high and the oxygen and carbon intensities are marginal. Hence, the EDS analysis indicates that silicon phases are predominant in the sample. Carbon present in the samples is completely oxidized. However, the observed small peak of carbon is caused by the presence of the silicon carbide phase and the presence of the oxygen peak indicates that oxides of silicon could be present. The XRD results confirm that the elemental carbon has completely disappeared, and silicon and silicon carbide are the only phases present in these samples after oxidizing the C/C-SiC ceramics. No indications of the presence of the oxides of silicon are found, confirming that neither silicon carbide nor free silicon oxidized during the process. The existence of free silicon is possible when it is covered by silicon carbide, which prevents its oxidation.

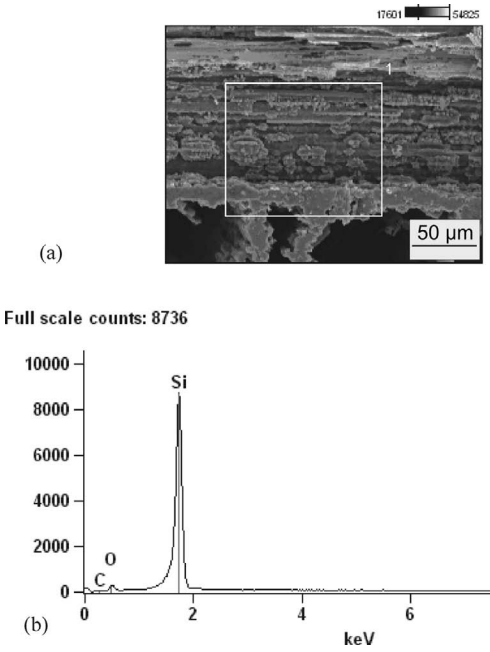

Fig. 7: EDS analysis of the oxidized-twill-weave, novolac-resin-derived C/C-SiC composite following oxidation at 1200 °C for 24 hours: (a) marked region of the analysis, (b) graph showing elements present in the sample.

After the complete oxidation of the carbon fibres, both fabric-derived composites show the same characteristics, e.g. a highly porous and uniform structure with the well developed SiC walls enclosing the pores (Figs. 8 and 9). The C-short fibre-reinforced composites differ in this respect significantly. After complete oxidation under the same oxidation conditions, a porous but random structure is created. Fig. 10 shows the random SiC wall arrangement, which is formed owing to the irregular fibre bundle arrangement of the short-fibre-derived ceramics. The pore sizes in the short-fibre case are smaller than in woven-fabric-based ceramics. Only a few thin SiC walls formed whereas a large number of siliconized single fibres are found.

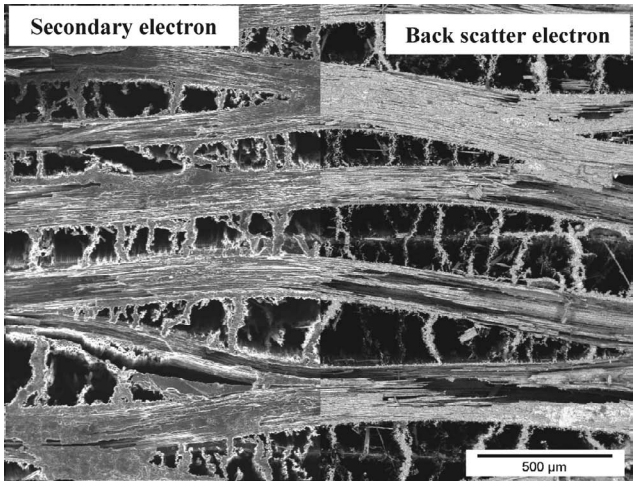

Fig. 8: SEM image showing the uniform, highly porous structure derived from oxidation of resol-resin, twill-weaved-based C/C-SiC composite.

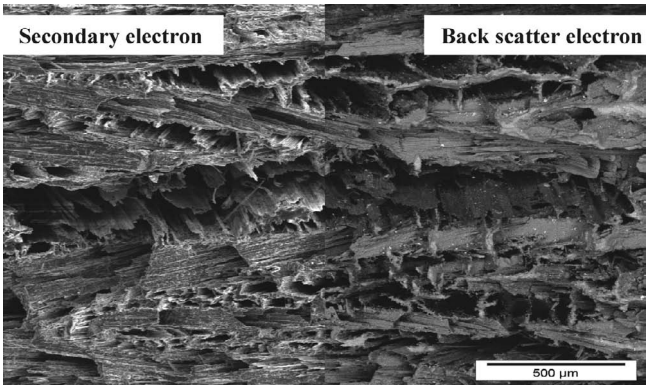

Fig. 9: SEM image showing the random structure derived from the oxidation of novolac-resin, short-fibre-weave-based C/C-SiC composite.

Fig. 10: A 3-D image reconstruction of a porous Si-SiC ceramic using computed tomography (novolac resin, twill-weave-derived).

Mercury porosimetry was applied to most of the samples. Samples corresponding to oxidation temperature of 1200 °C for 2 h duration are the best representatives to discuss. The pore size distribution for Si-SiC-ceramic derived from resol-resin, twill-weave fabric indicates (Fig. 11) the existence of a large number of pores in the range of 30 µm to 350 µm with an obtained open porosity of 70 %. Similar considerations are valid for novolac-derived, twill-weave composites and short-fibre-reinforced composites.

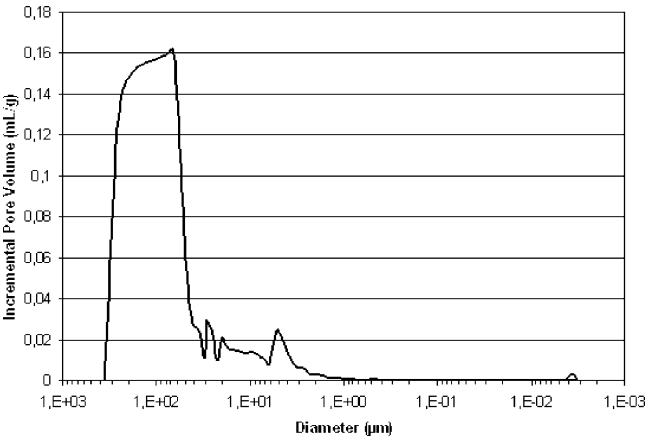

Fig. 11: Resol-resin, twill-weave-derived porous Si-SiC ceramic: Plot of incremental intrusion volume vs. pore diameter.

The EDX analysis of the composites subjected to the oxidizing temperature 1200 °C for 24 h shows the silicon phase predominantly present in the sample. The XRD analysis confirmed that only silicon and silicon carbide phases are present and did not show any indications of the presence of oxides of silicon.

The results were consistent when image analysis techniques like SEM and CT were used. The back scatter image in SEM showed silicon covered by silicon carbide. CT did not yield quantitative elemental results. However, a qualitative analysis showed well developed channels formed by the oxidation of carbon fibre tows.

(3) Modelling porosity

Si-SiC materials are useful in filter technology, as catalyst substrates, etc. There are demands for the modelling of the porosity of these new Si-SiC ceramics.

Assumptions:

i. Fibre tows/bundles are elliptical in shape (Fig. 12).
ii. Fibre tows/bundles are tortuously twisted (sinusoidal weave style) along their length in a woven-type pattern (Fig. 12).
iii. The Si-SiC walls divide the elliptical fibre tow/bundle into many blocks/segments and these Si-SiC walls are continuous in the sense that they run along the fibre tow/bundle length.
iv. The carbon matrix is assumed to be converted to silicon carbide during the siliconization stage with the result that all open porosity arises exclusively from the oxidation of carbon fibres.
v. The pores, forming independent channels, are separated by the Si-SiC walls as the fibre bundles had been previously separated from each other.

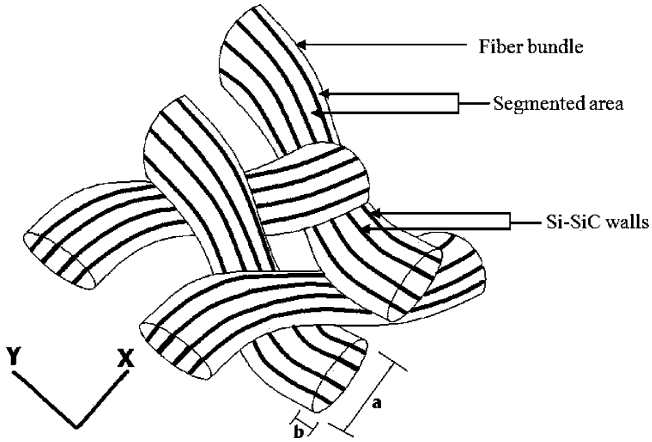

Fig. 12: Typical channels in the normal weave pattern which are formed by the oxidation of the segmented carbon fibre bundles.

For a two-dimensional, woven-fibre-reinforced composite, the total open porosity *'e'* is created by the oxidation of the woven-fibre tows/bundles. It consists of the open porosity created by removing the fibre/bundles extending along the x-direction and y-direction. It can be expressed by the equation,

$$e = e_x + e_y \quad (1)$$

Considering the fibres in the x-direction of a cuboid sample volume *'V'* of interest; the open porosity, arising from the complete oxidation of the carbon fibres, is the ratio of the total volume of the fibres in the sample to the total sample volume. The total fibre volume present in the x-direction of the sample is given by the product of the number of woven-fibre tows/bundles 'N_x' which represents the spacing between the fibre tow/bundles, the size of the

fibre tow/bundle described by the cross-sectional area of the fibre 'A_x' and the tortuous woven-fibre length 'l_x'; with the subscript '*x*' representing the x-direction weaving. Hence, the open porosity in the x-direction can be expressed mathematically as

$$e_x = \frac{\text{Total Fiber Volume}}{\text{Total Sample Volume}} = \frac{N_x \cdot A_x \cdot l_x}{V} \quad (2)$$

If 'A_{sx}' is the cross-sectional area and 'L_{sx}' is the length of the sample volume '*V*' in the x-direction, equation (2) can be simplified as

$$e_x = \frac{(n_x \cdot A_{sx}) \cdot (\frac{\pi}{4} \cdot a_x \cdot b_x) \cdot l_x}{(A_{sx} \cdot L_{sx})} \quad (3)$$

where 'n_x' is the number of fibre tows/bundles per unit cross-sectional area in x-direction
'a_x' and 'b_x' are the geometric diameters of the elliptical fibre tow/bundle in x-direction

Introducing two factors viz. scaling factor 'α_x' and tortuous factor 'β_x' for the fibre tow/bundle in the x-direction, we have

$$e_x = n_x \cdot \left(\frac{\pi}{4} \cdot a_x^2 \cdot \alpha_x\right) \cdot \beta_x \quad (4)$$

where

$$'\alpha_x' = \frac{b_x}{a_x}$$

$$'\beta_x' = \frac{l_x}{L_{sx}}$$

Similarly, the open porosity owing to the oxidation of the fibres along the y-direction can be written, analogous to equation (4), as

$$e_y = n_y \cdot \left(\frac{\pi}{4} \cdot a_y^2 \cdot \alpha_y\right) \cdot \beta_y \quad (5)$$

where all the terms hold their usual meaning for the y-direction

Substituting equations (4) and (5) in equation (1), the theoretical total open porosity obtained after oxidation is

$$e = \frac{\pi}{4} \cdot \left[\left(n_x \cdot a_x^2 \cdot \alpha_x \cdot \beta_x\right) + \left(n_y \cdot a_y^2 \cdot \alpha_y \cdot \beta_y\right)\right] \quad (6)$$

Generally, the fibre weaving along the x-direction and the y-direction has the same parameters. Further, from the images shown in Figs. 8 and 9 it can be seen Si-SiC walls are present within the fibre tow/bundle, which resembles the segmentation of the ellipse. Hence, an additional correction factor styled as segmentation factor 'γ' (<1) is incorporated into the above equation. Equation (6), therefore, becomes

$$e = \frac{\pi}{2} \cdot n \cdot a^2 \cdot \alpha \cdot \beta \cdot \gamma \quad (7)$$

where the terms represent for the x/y-direction

and tortuous factor 'β_x'

$= \frac{\pi}{2}$ – for semi-circular curve-based weaving

$= \frac{4}{\pi}$ – for cycloid curve based weaving

$= 1.216006$ – for sinusoidal curve based weaving

The number of pores per unit of cross-sectional area can be estimated using the micrographs and depends on the carbon-fibre fabric size, fibre stacking arrangement, fibre spacing, etc. The geometric dimensions of the elliptical fibres can be calculated from the carbon-fibre-fabric manufacturer data sheet. The value of 'γ' is typically in the range of 0.90 to 0.98. For the sample as shown in Fig. 8 (Si-SiC ceramic derived from twill-weave carbon fabric and resol-resin-based C/C-SiC composite) and assuming sinusoidal curve-based weaving with the $n = 1.8\ mm^{-2}$ estimated from the optical micrographs, the major axis of the pore approximated to the ellipse is $a = 1.2\ mm$, scaling factor $\alpha = 0.1667$ and taking the segmentation factor as $\gamma = 0.95$, we have the theoretical open porosity of the Si-SiC ceramic calculated using equation (7) as:

$$e = \frac{\pi}{2} \times \left(1.8\ \text{mm}^{-2}\right) \times (1.2\ \text{mm})^2 \times 0.1667 \times 1.216006 \times 0.95 \quad (8)$$

$$e = 0.7840 \text{ or } 78.40\% \quad (9)$$

The theoretical open porosity obtained in equation (9) is consistent with the experimental result for the ceramic under consideration as shown in the graph marked as Fig. 3 following complete oxidation of the fibres, which has taken place at 1200 °C when held for 2 h.

(4) Model for pore size distribution

The pore size distribution in the Si-SiC ceramic is modelled by applying statistical theory. The model is derived taking into assumption that after oxidation the segmented elliptical fibre tow/bundle results in the elliptical porous channel segmented by Si-SiC walls with each of these segments being approximated to rectangular-shaped pores as shown in Fig. 13.

The approximated rectangular pore segments have to be modelled for two characteristic dimensions, viz. length and breadth of the rectangle. The following are the characteristics of these rectangular pores that have to be considered while choosing the probability distribution.

i. The characteristic dimension '*d*' of the pores is an entity of continuously varying and unpredictable size (continuous random variable).
ii. These rectangular pores occur in a countably infinite number with their widths being distributed over one or more continuous intervals of the real line.
iii. The pores are mutually independent, i.e. the occurrence of one pore does not influence the other, and disjointed.
iv. The characteristic dimension '*d*' remains unchanged over time.
v. The characteristic dimension '*d*' can take only finite positive values

A distribution adequate to describe the characteristic dimension '*d*' of the pores is the gamma distribution [14]. A two-parameter gamma distribution can be defined using shape parameter 'α' and scale parameter 'β' in the domain $[0,+\infty]$ as

$$f(x,\alpha>0,\beta>0) = \frac{x^{\alpha-1}}{\beta^{\alpha} \cdot \Gamma(\alpha)} \cdot \exp\{-\frac{x}{\beta}\} \quad (10)$$

and $\Gamma(\alpha)$ is a gamma function of α, which is defined by

$$\Gamma(\alpha) = \int_0^{\infty} u^{\alpha-1} \cdot \exp\{-u\} \cdot du \quad (11)$$

The values of 'α' and 'β' are estimated for each of the characteristic dimensions with the maximum likelihood estimation (MLE) technique. An approximate value of the shape parameter 'α' is found using the following expression (statistical mathematics),

$$\alpha \approx \frac{3 - s + \sqrt{(s-3)^2 + 24s}}{12s} \quad (12)$$

where

$$s = \ln\left(\frac{1}{m}\sum_{i=1}^{m} d_i\right) - \frac{1}{m}\sum_{i=1}^{m} \ln(d_i) \quad (13)$$

and 'd_i' is the linear dimension of the 'i' pore such that $i = 0, 1, 2, \ldots, m$.

The maximum likelihood estimate for the scale parameter 'β' is given by

$$\beta = \frac{1}{\alpha m}\sum_{i=1}^{m} d_i \quad (14)$$

The values of 'α' and 'β' being known, the mean characteristic dimension 'd' of the rectangular pores can be calculated using the equation

$$d = \bar{x} = \alpha\beta \quad (15)$$

The above model is simulated by using the software package (Easy-fit), which fits various distributions to the given data using the MLE technique. The raw input data for Easy-fit are the data obtained from the mercury intrusion porosimetry test. The model was derived taking into consideration that the segmented pores are rectangular in shape; however, the pore shapes are not distinguished in the mercury intrusion porosimetry test as they are approximated to be circular/cylinder. Hence, the simulation is performed taking pore diameter as the variable ('x'). The probability densities corresponding to each pore diameter are equivalent to the incremental mercury intrusion volume automatically normalized by Easy-fit to sum up to unity (representing the area under the density curve). Any negative probability density values are of no relevance because, as a result of removing the pressure, the mercury leaks out of the penetrated pore. The data are then fitted to a two-parameter gamma distribution using MLE technique.

Simulating the mercury intrusion porosimetry test data of the novolac resin, twill-weave-fabric-derived porous Si-SiC ceramic and fitting two-parameter gamma distribution, the fit shown in Fig. 14 is obtained with the values of the parameters as $\alpha = 1.6$ and $\beta = 65.0$ µm. Hence, from equation (15), the mean pore diameter is $d = 104$ µm. This value has good coherence with that of the results obtained with the mercury intrusion porosimetry, thus confirming the validity of the model.

Easy-fit also calculates and gives values for the following parameters:

- Mean diameter = 1.E+2 µm
- Variance = 6.8E+3 µm
- Standard deviation = 82.0 µm
- Coefficient of variance = 0.79
- Skewness = 1.6; measure for the asymmetry of the distribution of a random variable like the pore width. At a positive skew for pore width, small-sized pores dominate whereas at negative skew, large pore widths dominate.
- Kurtosis = 3.7; measure for the shape of the distribution of a random variable by the width of the distribution, i.e. the range of pore widths that occur.

A mathematical model for open porosity is developed and validated by comparing the results from the model with those obtained from experiments/tests. A statistical model for the pore size distribution is also established wherein the characteristic pore dimensions are fitted using the two-parameter gamma distribution. This statistical model is simulated in the Easy-fit software package and the model is validated with the data obtained from mercury intrusion porosimetry tests.

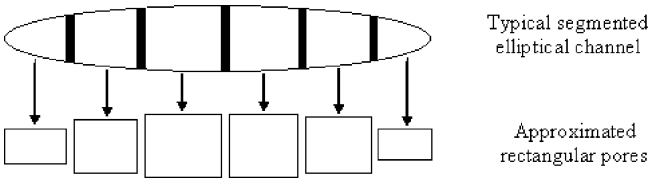

Fig. 13: A segmented elliptical channel shown approximated to rectangular pore.

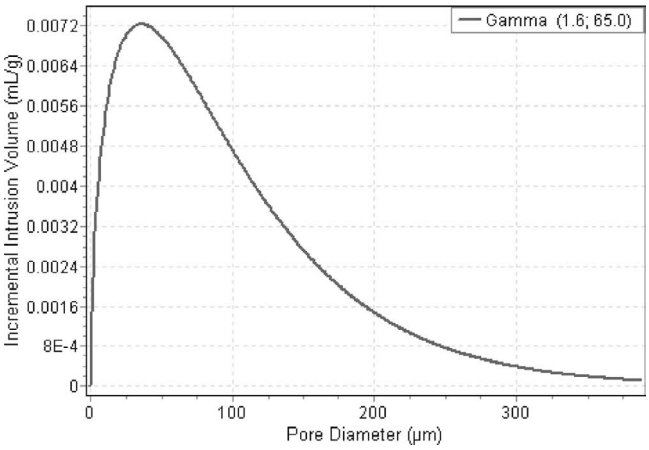

Fig. 14: Two-parameter gamma distribution fitted for the mercury intrusion porosimetry test's data for the novolac resin, twill-weave-derived porous Si-SiC ceramic.

Concluding, the oxidation of the C/C-SiC composite resulted in complete oxidation of carbon, thus obtaining well developed channels running throughout the composite, which could have potential applications as a porous material. The open porosity obtained was appreciably high with a pore sizes distributed around 150 µm. There is, however, potential for improvement by modifying the fibre matrix bonding in order to obtain a particular type of porous ceramic to suit a specified application.

IV. Conclusions

The factors influencing porosity are discussed and it is found that the fibre arrangement, the phenolic resin type, temperature of oxidation and the holding times significantly influence the mass losses and the obtained level of open porosity. Woven fabrics are preferred as they are ordered structures and the pores formed are more uniform with the network of pores. They are well developed in comparison to the pores in case of short fibres. Also, the resol-derived

phenolic resins used here created uniform and symmetrical SiC wall structures formed within the fibre bundle. The Novolac-resin-based composites used in this work show a less well organized structure. Furthermore, the oxidation temperature has a pronounced effect on the mass loss and open porosity up to around 900 °C. The change in porosity can be inversely related to change in mass.

The open porosity and its pore size distributions are determined using a helium-gas pycnometer, the Archimedes method and mercury porosimetry. The results obtained with these three methods agreed well within the experimental limits of accuracy. Mercury porosimetry showed that most of the pores had diameters in the range of 20 µm to 300 µm for different samples. The models developed in this work describe the open porosity and its distribution in the Si-SiC ceramic material in accordance with the experimental results.

Acknowledgements:

We wish to thank Dipl.-Ing. Ingrid Otto, Department of Material Processing Engineering, University of Bayreuth, Germany for helping us perform experiments related to mercury intrusion porosimetry and other analyses.

References

1 Krenkel, W.: From Polymer to Ceramics: Low Cost Manufacturing of Ceramic Matrix Composite Materials, *Mol. Cryst. and Liq. Cryst.*, **354,** [1], 353 – 364, (2000).

2 Zawada, L.P., Hay, R.S., Lee, S.S., Staehler, J.: Characterization and High-Temperature Mechanical Behavior of an Oxide/Oxide Composite, *J. Am. Ceram. Soc.*, **86,** [6], 981 – 990, (2003).

3 Levi, C.G., Yang, J.Y., Dalgleish, B.J., Zok, F.W., Evans, A.G.: Processing and Performance of an All-Oxide Ceramic Composite, *J. Am. Ceram. Soc.*, **81**, [8], 2077 – 2086, (1998).

4 Levi, C.G., Zok, F.W., Yang, J.Y., Mattoni, M., Löfvander, J.P.A.: Microstructural Design of Stable Porous Matrices for All-Oxide Ceramic Composites, *Z. Metall.*, **90,** [12], 1037 – 1047, (1999).

5 Weiss, R.: Carbon-Fibre-Reinforced CMCs: Manufacture, Properties, Oxidation Protection, in: *High Temperature Ceramic Matrix Composites*, WILEY-VCH, Weinheim, Germany, 440 – 456, (2001).

6 Christin, F.: Design, Fabrication and Application of Thermostructural Composites (TSC) like C/C, C/SiC and SiC/SiC Composites, *Adv. Eng. Mater.*, **4**, [12], 903 – 912, (2002).

7 Kochendörfer, R., Lützenburger, N.: Applications of CMCs made via the Liquid Silicon Infiltration (LSI) Technique, in: *High Temperature Ceramic Matrix Composites*, WILEY-VCH, Weinheim, Germany, 277 – 287, (2001).

8 Labanti, M., Martignani, G., Mingazzini, C., Minoccari, G.L., Pilotti, L., Ricci, A., Weiss, R.: Evaluation of Damage by Oxidation Corrosion at High Temperatures of Coated C/C-SiC Ceramic Composite, in: *High Temperature Ceramic Matrix Composites*, WILEY-VCH, Weinheim, Germany, 218 – 223, (2001).

9 Hillig, W.B., Mehan, R.L., Morelock, C.R., DeCarlo, V.I., Laskow, W.: Silicon/Silicon Carbide Composites, *Am. Ceram. Soc. Bull.*, **54**, [12] (1975).

10 Krenkel, W.: Cost Effective Processing of CMC Composites by Melt Infiltration (LSI-Process), *Ceram. Eng. Sci. Proc.*, **22**, [3], 443 – 454, (2001).

11 Schulte-Fischedick, J., Zern, A., Mayer, J., Rühle, M., Friess, M., Krenkel. W., Kochendörfer, R.: The Morphology of Silicon Carbide in C/C-SiC Composites, *J. Mater. Sci. Eng. A*, 146 – 152, (2002).

12 Krenkel, W., Renz, R., Heidenreich, B.: Lightweight and Wear Resistant CMC Brakes, In: *Ceramic Materials and Components for Engines,* WILEY-VCH, Weinheim, Germany, 63 – 67, (2001).

13 Krenkel, W.: Designing with C/C-SiC Composites, in: *Advances in Ceramic Matrix Composites IX*, *Ceram. Trans.*, **153**, 103 – 123, (2003).

14 Soong, T. T.: *Fundamentals of Probability and Statistics for Engineers*, John Wiley & Sons, Ltd., (2004).